

5-D Force Control System for Fingernail Imaging Calibration

Yun Lin and Yu Sun

Abstract—This paper presents a low-cost automated system that is able to apply a 5-degree-of-freedom (DOF) force on a human fingertip with high precision. It is designed to be used as a calibration platform for the previous proposed fingernail imaging system, and as a haptic system. The system is composed of two Novint Falcon devices linked by two universal joints and a rigid bar to provide 5-DOF motion and force, with feedback from a 6-DOF force sensor. A force controller is designed with an inner position control to meet the calibration goal and requirement. Experiment result and analysis showed that the system was capable of controlling the force with a settling time of less than 0.25 seconds. Two force trajectories are designed for fast and sufficient calibrations. A calibration experiments demonstrated that the system tracked the trajectories with an interval of 0.3 seconds, and step sizes of 0.1 N and 1 N-mm with root-mean-squared errors of 0.02 - 0.04 N for forces and 0.39 N-mm for torque.

I. INTRODUCTION

Previously in [10], a camera-based finger force imaging system was designed to detect the fingertip force by measuring the coloration of the fingernail and surrounding skin. The finger force imaging system could measure normal and shear forces with an accuracy of 5–10% for a force range of up to 8 N. A difficulty with our previous work [10], [9] is that building accurate mathematical models involves an extensive calibration for each individual subject.

Originally, in [9] and [5], the calibration was controlled by the human subjects, who read the force by visual feedback from a force sensor placed under the fingerpad, and adjust their finger toward the desired force in multiple axes. In order to minimize the training time, a training trajectory was devised to cover the feasible force space. However, no matter how effective the visual feedback is, it is a difficult task for the human subjects to control three variables simultaneously. Also, as long as the humans act in a subjective way, it is fatiguing for the human subject to apply forces for an extended amount of time, especially for repeated training sessions. Finally, if we consider more variables than 3-axis force in training session, it would become impractical to rely on the humans to control more than 3 variables simultaneously.

To have the calibration carried out efficiently and automatically, a passive 3-degrees-of-freedom (DOF) force calibration platform was designed in [3], which was composed of a 6-DOF Butterfly Magnetic Levitation Device (Maglev) and a 6-axis ATI Nano 17 force sensor. By using both position and force loop, the device could apply desired calibration

Yun Lin and Yu Sun are with the Department of Computer Science and Engineering, University of South Florida. (yunlin@mail.usf.edu, yusun@cse.usf.edu)

force in normal and shear directions on the fingerpad. With the system, the human subjects could rest their fingers in a finger restraint and reply on the system to apply proper force.

Although the Butterfly Maglev device has three rotational degrees of freedom that could be controlled, the angular motion ranges of the current system are too small to be used to apply enough torques on fingertips, since the elastic property of the fingertip skin presents large deformation to respond the torques. With ± 8 degrees for all three directional rotations [1], [2], the Maglev device can only apply up to around 10 N-mm torque which is far less than a typical torque of 70 N·m used in many research studies [4]. Besides, even though the Butterfly Maglev device is an advanced research tool that plays a center role in many studies and applications, its high price tag (50,000 USD) prevents it from being used widely as a low-cost calibration tool.

This paper presents a new calibration stage design that consists of two Novint Falcon devices and a ATI Nano 17 force sensor. The Novint Falcon device costs less than 200 USD each. We are able to control the two Falcon devices with the force and torque feedback to output desired 3-DOF force and 2-DOF torque with root-mean-squared errors of 0.02 - 0.04 N for forces and 0.39 N-mm for torques. Our system have ± 20 degrees of rotation range for two axes, which allow it to apply torque range from -3.2 N·m to 3.2 N·m theoretically. Besides the application in our force imaging system, this calibration platform can also be used in some haptic applications.

In section II, this paper describes the design of the new calibration system. In section III, the whole control strategy design, implementation and experimental validation of the control design are introduced. In section IV, force trajectories are designed, and the successful tracking of force trajectories for calibration of the fingernail imaging system is demonstrated.

II. SYSTEM DESIGN

As illustrated in Figure 1, human fingers are able to generate six directional forces and torques. When a finger presses against a surface, it performs a positive normal force F_z ; when the finger has relative shifting in x and y directions, it generates frictional shear forces F_x and F_y ; when the finger rotates around the axes x, y and z anticlockwise, it creates positive rotational torques T_x , T_y and T_z .

The design of calibration system is shown in Figure 2. Two Novint Falcon devices are used in this system [7]. The end effector of each Novint Falcon has three degrees of freedom, a workspace of $4' \times 4' \times 4'$ ($101.6 \times 101.6 \times 101.6$ mm 3), and a force capability of 2 lbs, approximately

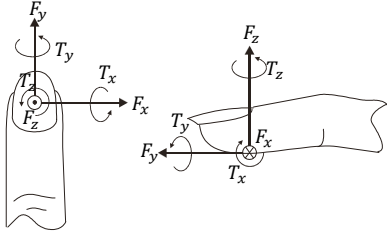


Fig. 1. The directional definition of applied forces when finger is touching against a surface. Axis z points to the direction that is perpendicular to the surface of fingerpad, axis y points out along the fingertip, and axis x is perpendicular to axes y and z.

8.8 N. In order to generate more than 3-axis forces, the end-effectors of both devices are removed and a bar with one universal joints at each end is designed and connected to the Falcon devices to keep the linear motion, which adds two directions of rotational motion. So, together the midpoint of the bar has 5-DOF. Based on the specification of the Falcon system and forward kinematics (Section III-B), the integrated calibration system has a workspace of $4' \times 4' \times 4'$, and a rotation of $\pm 20^\circ$ in horizontal and vertical directions. This calibration platform should be able to produce forces from -16 N to 16 N in x and y directions, and -18 N to 10 N in z direction considering gravity. It can also generate both horizontal and vertical torques with a range from -3.2 N·m to 3.2 N·m theoretically, which is far beyond the torque range of ± 70 N·mm that the humans regularly perform [4].

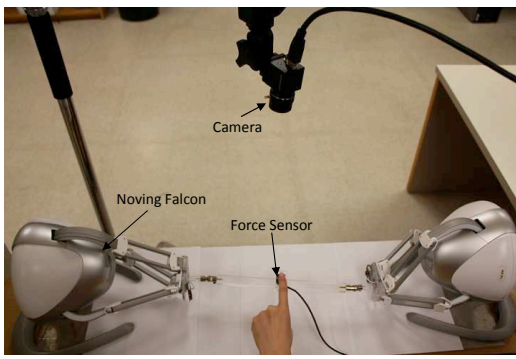


Fig. 2. The proposed calibration stage that is capable to apply a 5-DOF force on a human fingerpad.

For calibration and feedback purpose, a 6-axis ATI Nano 17 force/torque sensor is attached to the middle of the bar to measure the fingerpad force in 6-axis. A plastic flat plane is mounted on the ATI Nano 17 force sensor to provide a contact surface. A Point Grey Flea video camera is mounted above the middle of the bar to capture the finger images.

The whole system is controlled by one PC to run both force controller and position controller at a 1KHz sampling rate. The force sensor data are filtered and amplified by an amplification box and read using the A/D inputs on a Sensoray 626 data acquisition board installed in the PC. The camera takes images at 30 Frame-per-second (fps).

III. CONTROL DESIGN

A control strategy is designed to minimize force errors, response time, calibration time, and ensure system stability[6]. The controller block diagram is shown in Figure 3. The inputs of the whole system are 5-D desired forces. We use a force controller as an outer loop with two inner position loops for two Novint Falcon devices (FD). The desired position X_d is calculated by force controller, and then it is decoupled through inverse kinematics into the desired position X_{1d} , X_{2d} of Falcon devices FD1 and FD2. The position loops of both Falcon devices control each FD to its desired position. The applied forces on fingertip are transformed through forward kinematics and finger model.

A. System Model

There are two unknown models in the system, finger dynamics and FD model. In previous works, the finger dynamics have been modeled as a linear approximation, since our force range is small. The finger stiffness K_f is estimated at $1200N/m$ and the finger damping b_f is estimated at $5 N/(m/s)$ [3].

FD model is estimated for position controller design. Since the FD is a 3-DOF system and has its own kinematics, it is treated as a black box system. The inputs are 3-D desired forces, and the output is the position of its end-effector. In order to keep the output in its workspace without bumping the boundary, the periodical pulse inputs were applied to the force, as shown in Figure 4. The response was measured and divided into two parts. The first part is used as estimation data, and the second part is specified as validation data. We identified it as a second order underdamped system in Equation 1.

$$k_p \frac{\omega_n^2(1+T_z)}{s^2 + 2\zeta\omega_n s + \omega_n^2} = k_p \frac{(1+T_z s)}{T_w s^2 + 2\zeta T_w s + 1} \quad (1)$$

The models in x, y, and z axes can be identified as one. The identification results are $K = 0.0288$, $T_w = 0.1312$, $\zeta = 0.2940$, and $T_z = -0.0147$. Figure 5 shows the output of simulated model in y direction, compared with measured validation data. The identified model matches the real dataset with accuracies of 87.35%, 86.56% and 86.98% in axes x, y and z.

B. Kinematics

A set of coordinate frames are built for kinematic analysis. As illustrated in Figure 6, we choose the base coordinate frame $o_0x_0y_0z_0$ of FD1 as the base of whole system. The base coordinate frame of FD2 is denoted by $o'_0x'_0y'_0z'_0$. Then the frames $o_1x_1y_1z_1$, $o_2x_2y_2z_2$ are attached to the end effectors of FD1 and FD2 respectively, and the frame $o_3x_3y_3z_3$ is attached to the midpoint of the link. The distance between these two coordinate frames $o_0x_0y_0z_0$ and $o'_0x'_0y'_0z'_0$ is $d(d_1, d_2, d_3) = (292mm, 6mm, 0)$. The length of the link is $l = 282$ mm. Because the coordinate Frames $o_1x_1y_1z_1$, $o_2x_2y_2z_2$ and $o_3x_3y_3z_3$ are on the same link, they have the same rotation. Therefore the positions and rotations of coordinate frame $o_i x_i y_i z_i$ ($i = 1, 2, 3$) related to $o_0x_0y_0z_0$ can be denoted by $(a_i, b_i, c_i, \beta, \gamma)$. a_i ,

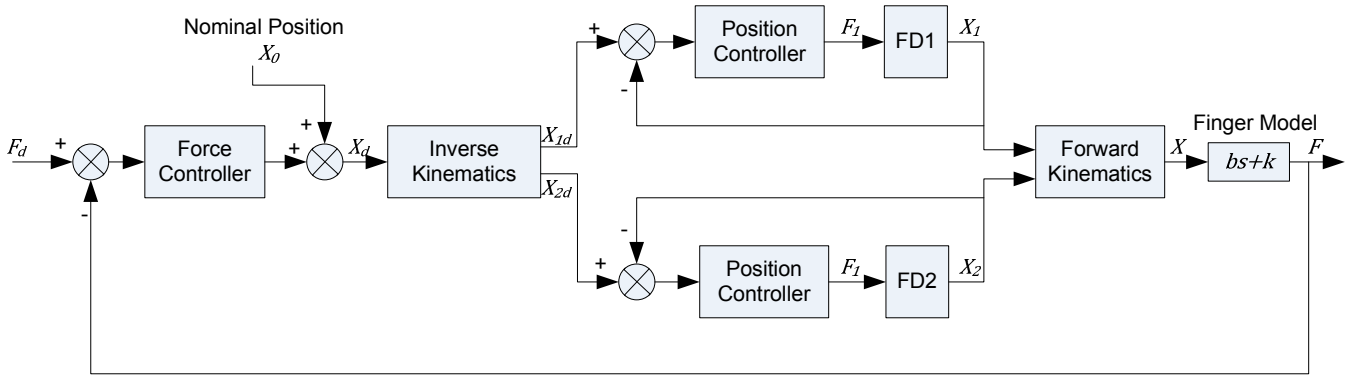


Fig. 3. Block diagram of the force controller showing inner position loop and outer force loop.

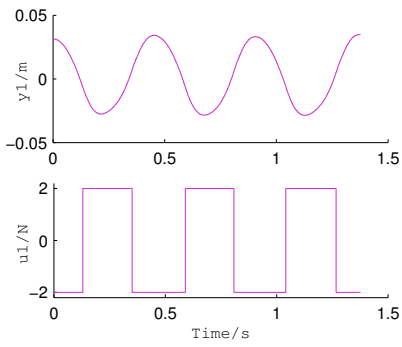


Fig. 4. Measured data used for system identification. \$u_1\$ is the input and \$y_1\$ is the output.

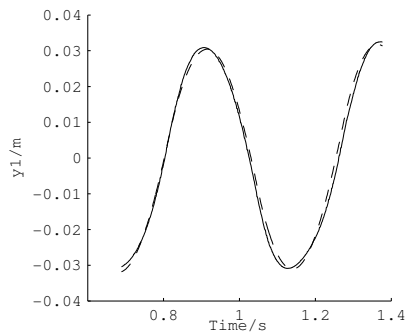


Fig. 5. The measured output compared with simulated output of the model in y direction. The measured output is shown as dashed lines and the simulated output is shown as solid lines.

\$b_i, c_i\$ denote the position of each coordinate frame. \$\beta\$ denotes the angle that the coordinate frames rotate around its axis of \$y_i\$ about the axis of \$y_0\$, and \$\gamma\$ denotes the angle that the coordinate frames rotate around its axis of \$z_i\$ about the axis of \$z_0\$. The link rotates around the z-axis for \$\gamma\$, and then rotates around the y axis for \$\beta\$. Thus, the transformation matrix of each coordinate system can be expressed in Equation 2 and 3. For convenience, we use \$c(\gamma)\$ and \$s(\gamma)\$ which denote \$\cos(\gamma)\$ and \$\sin(\gamma)\$ respectively.

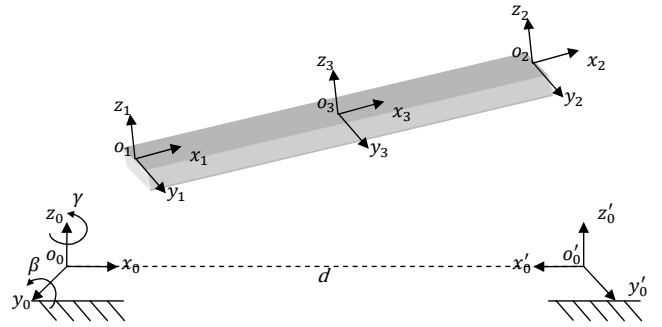


Fig. 6. Kinematics of the system

$$T_1^0 = H_1^0 R_{z,r} R_{y,\beta} \\ = \begin{bmatrix} c(\beta)c(\gamma) & -s(\gamma) & c(\gamma)s(\beta) & a_1^0 \\ c(\beta)s(\gamma) & c(\gamma) & s(\gamma)s(\beta) & b_1^0 \\ -s(\beta) & 0 & c(\beta) & c_1^0 \\ 0 & 0 & 0 & 1 \end{bmatrix} \quad (2)$$

where \$T\$ is the transformation matrix, and \$H\$ is the homogeneous transformation matrix. We use a notation in which a superscript and a subscript are used to denote the reference frame and the current frame. For example, \$T_j^i\$ is the transformation matrix of \$o_j x_j y_j z_j\$ related to \$o_i x_i y_i z_i\$. \$R_{z,\gamma}\$ is the rotation matrix around z-axis, and \$R_{y,\beta}\$ is the rotation matrix around y-axis.

$$T_3^0 = H_1^0 T_3^1 \\ = \begin{bmatrix} c(\beta)c(\gamma) & -s(\gamma) & c(\gamma)s(\beta) & a_1^0 + \frac{l}{2}c(\beta)c(\gamma) \\ c(\beta)s(\gamma) & -c(\gamma) & s(\gamma)s(\beta) & b_1^0 + \frac{l}{2}c(\beta)s(\gamma) \\ -s(\beta) & 0 & c(\beta) & c_1^0 - \frac{l}{2}s(\beta) \\ 0 & 0 & 0 & 1 \end{bmatrix} \quad (3)$$

The inverse kinematics of \$o_1 x_1 y_1 z_1\$ is derived from Equation 3, as depicted in Equation 4. The variables \$a_3^0, b_3^0, c_3^0, \beta, \gamma\$ are the output of the outer force controller.

$$\begin{cases} a_1^0 = a_3^0 - \frac{l}{2}c(\beta)c(\gamma) \\ b_1^0 = b_3^0 - \frac{l}{2}c(\beta)s(\gamma) \\ c_1^0 = c_3^0 + \frac{l}{2}s(\beta) \end{cases} \quad (4)$$

Similarly, the inverse kinematics of $o_2x_2y_2z_2$ is

$$\begin{cases} a_2^0 = a_3^0 + \frac{l}{2}c(\beta)c(\gamma) \\ b_2^0 = b_3^0 + \frac{l}{2}c(\beta)s(\gamma) \\ c_2^0 = c_3^0 - \frac{l}{2}s(\beta) \end{cases} \quad (5)$$

The position of $o_2x_2y_2z_2$ in the basic coordinate frame needs to be converted to the position in its own coordinate systems $o_0'x_0'y_0'z_0'$ through forward kinematics, as expressed in Equation 6.

$$T_2^{0'} = T_0^{0'} T_1^0 T_2^1 \\ = \begin{bmatrix} -c(\beta)c(\gamma) & s(\gamma) & -c(\gamma)s(\beta) & d1 - a_1^0 - lc(\beta)c(\gamma) \\ -c(\beta)s(\gamma) & -c(\gamma) & -s(\gamma)s(\beta) & d2 - b_1^0 + lc(\beta)s(\gamma) \\ -s(\beta) & 0 & c(\beta) & d3 + c_1^0 - ls(\beta) \\ 0 & 0 & 0 & 1 \end{bmatrix} \quad (6)$$

From Equation 4 and Equation 6, the position of $o_2x_2y_2z_2$ correlated to the coordinate fram $o_0'x_0'y_0'z_0'$ is:

$$\begin{cases} a_2^{0'} = d_1 - a_3^0 - \frac{l}{2}c(\beta)c(\gamma) \\ b_2^{0'} = d_2 - b_3^0 - \frac{l}{2}c(\beta)s(\gamma) \\ c_2^{0'} = d_3 + c_3^0 - \frac{l}{2}s(\beta) \end{cases} \quad (7)$$

From the technical specification of the Novint Falcon, the workspace of $o_1x_1y_1z_1$ related to $o_1x_1y_1z_1$ and the workspace of $o_2x_2y_2z_2$ related to $o_0'x_0'y_0'z_0'$ are both $([-50mm, 50mm], [-50mm, 50mm], [-50mm, 50mm])$. Therefore, the workspace of $o_2x_2y_2z_2$ and $o_3x_3y_3z_3$ in the base coordinate frame can be derived from the Equation 4, 5 and 7. The workspace of $o_2x_2y_2z_2$ is $([242mm, 342mm], [-44mm, 56mm], [-50mm, 50mm])$, and the workspace of $o_3x_3y_3z_3$ is $([96mm, 196mm], [-47mm, 53mm], [-50mm, 50mm])$. $\beta \in [-19.5^\circ, 21.8^\circ]$, $\gamma \in (-20.77^\circ, 20.77^\circ)$.

C. Controller Design

A PID controller is used in the inner position loop as $K_p + \frac{K_i}{s} + K_d s$ for all three directions x, y and z. The PID parameters need to be tuned to achieve a robust and fast responding system. The root locus method is used to help choose suitable parameters for the Novint Falcon devices which have been identified as a second order underdamped system in previous subsection. The root locus of the inner loop is shown in Figure 7. The desirable gains are chosen from the root locus as $K_p = 132$, $K_d = 5.148$. The root locus method provides a start point for gain tuning. But the actual desirable gains have to be experimentally tuned due to uncertainty in dynamics. Eventually we found by experiments that $K_p = 120 \text{ m}\cdot\text{s}/N$, $K_d = 0.3 \text{ m}/N$, and $K_i = 1.32$ that reduces the static errors resulted in optimal performance for all three axes. The derivative term deviates a lot from the root locus result, and we introduced integral term, because we want to eliminate system oscillation.

The outer force loop also used a PID controller as $K_f + \frac{K_i}{s} + K_{vs}$. Root Locus methods are no longer applicable for tuning gains of the outer force loop because it is difficult to obtain such a complicated model for the 5-axis force

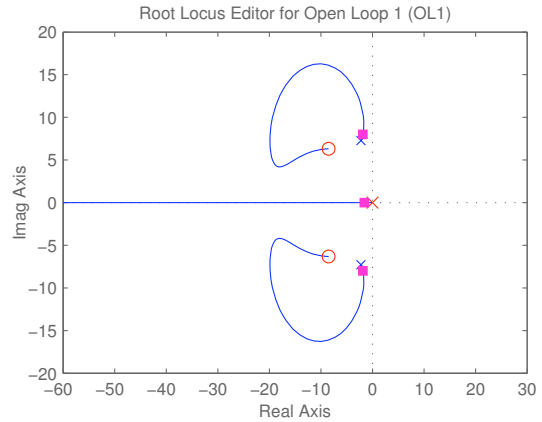


Fig. 7. Root Locus of the position controller.

controller, which involves inverse kinematics and the whole inner position loops of both FDs, the midpoint position coupled by forward kinematics, and finger dynamics. A minor error of each part would lead to huge errors of the whole system. Instead, the gains of the outer force loop in five axes are directly tuned through experiments, in which Ziegler-Nichols method are applied. The final gains are $K_f = 0.00055 \text{ m}\cdot\text{s}/N$, $K_i = 0.00045 \text{ m}/N$ for forces F_x , F_y and F_z , and $K_f = 0.01 \text{ m}\cdot\text{s}/N$, $K_i = 0.0001 \text{ m}/N$ for torques. The nominal position X_0 represents the desired nominal position at which forces will be applied. The desired position is calculated as: $X_d = X_0 + \Delta P$.

D. Experimental Results of the Controller

To evaluate the control design, a step input of 1N desired force was applied in turn to each of the three force directions, and a step input of 10 N·m torque was applied in Z axis. The response of F_z is shown in Figure 8. The response is stable and has a settling time of 0.3 seconds. The response of F_x and F_y are similar to that of F_z , with a faster settling time of approximately 0.2 seconds. Figure 8 also shows good disturbance rejection by the x- and y-axis controller in response to a step input in z. The forces in all three directions have a steady state RMSE (Root Mean Squared Errors) of approximately 0.03 N, and the torque in z direction has a steady state RMSE of 0.2 N·m.

The response of T_z is shown in Figure 9. The settling time is 0.2 seconds. Note that T_x and T_y were not controlled. The system applies a 5-DOF force except the Torque in x direction. T_y was not controlled either because a tiny error in T_y would lead to a large error in the desired position, which results in a big rotation around y-axis.

IV. TRAJECTORY DESIGN AND RESULTS

The calibration trajectories need to be designed so that a rich set of training data is collected over the entire force space. The system has the ability to control 5-DOF forces simultaneously. Theoretically, the trajectory should be designed to cover the whole 5-DOF force space. However, the torque T_y which rotates around the y-axis has tremendous influence on system stability, because a tiny error of T_y will

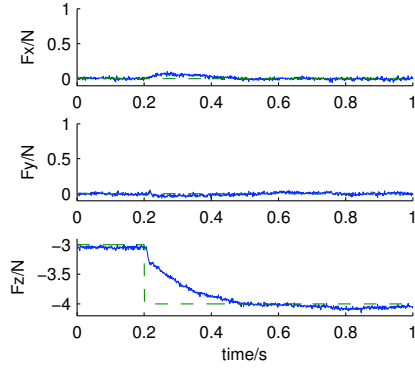


Fig. 8. Z-direction force step response. The desired force trajectory is shown as dashed lines and the measured force on the finger pad is shown as solid lines.

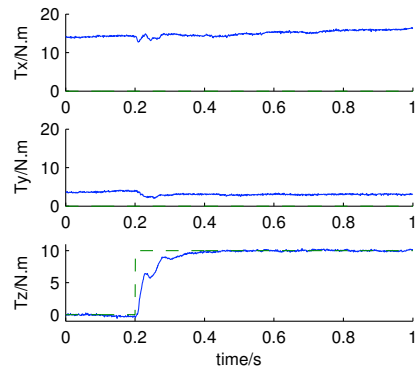


Fig. 9. Z-direction Torque step response. The desired force trajectory is shown as dashed lines and the measured force on the finger pad is shown as solid lines.

lead to a big rotation around y-axis. If the finger is a little off center from the sensor, it will lead to large error in the rotation as well. In other words, the control of T_y focuses more on the contact surface where the finger presses against a plane. Therefore, in order to guarantee the system stability, we control 4-D forces, which are shear forces F_x , F_y , normal force F_z and the torque T_z . The 4-D forces are of the most interest in many tasks such as one holding a pen without letting it rotate.

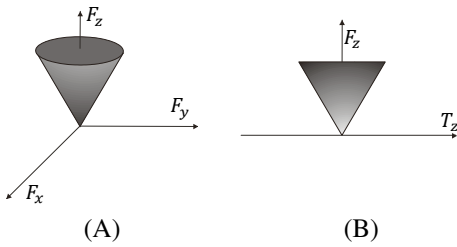


Fig. 10. (A) Force Constraints in the space of F_x , F_y and F_z . (B) Force Constraints in the area of F_z and T_z .

The feasible force space is constraint by maximal static frictional coefficient. The maximum shear force F_x , F_y and the torque T_z are constraint by maximum normal force F_z .

The feasible spaces are depicted in Figure 10 (A) and Figure 10 (B), which show a 3-D cone in the space of F_x , F_y , F_z , and an triangle in the area of F_z and T_z . As the sampling space increases by one dimension, the sampling complexity is increased exponentially. It would take hours for the desired trajectory to cover the whole 4-D space with a step size 0.1 N in its feasibles force space.

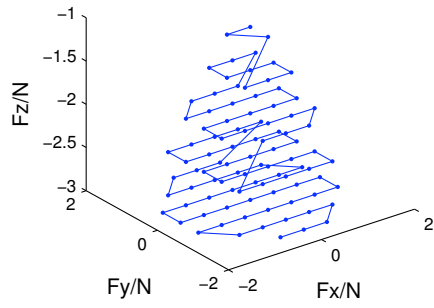


Fig. 11. A force trajectory generated in the space of F_x , F_y and F_z .

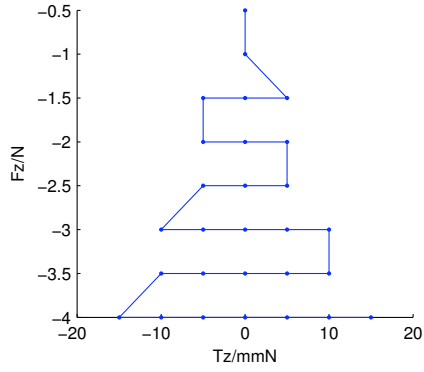


Fig. 12. A force trajectory in the area of F_z and T_z

Instead, we design two trajectories, as shown in Figure 11 and Figure 12. To prevent sliding, the contacted plane in experimental platform is covered with a tape. The usual static coefficient of friction of is approximately 0.6, and the usual static coefficient of friction of torque and normal force is 4 mm [4]. Therefore, if the normal force ranges between 0 and 3 N, the total shear force can range between 0 and 1.8 N, and the total torque in z direction ranges between 12 N·mm. The training data designed in either cylindrical coordinators or Cartesian coordinates. We design the trajectory in Cartesian coordinates.

A set of waypoints with a step size of 0.1 N in forces and 1 N·mm in torques are generated over the Cartesian coordinate space. Then the force trajectory is designed in a shortest way to transpose all the waypoints one by one. Additionally, the forces ramp up to each waypoint in 0.1 seconds and hold the data point for 0.2 seconds, the time for camera to take pictures. Figure 13 and Figure 14 show the tracking results

of force trajectories. The RMSE is 0.04 N in F_x , 0.02 N in F_y , 0.03 N in F_z , and 0.39 N·mm in T_z .

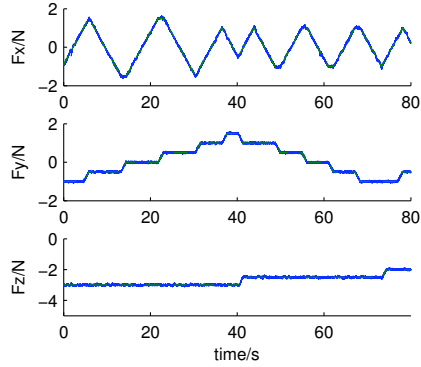


Fig. 13. Force tracking in F_x , F_y , F_z space.

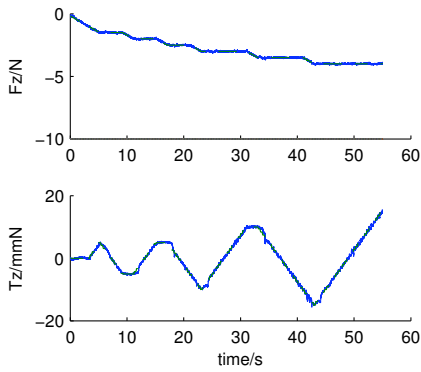


Fig. 14. Force tracking in T_z and F_z area.

V. DISCUSSION AND FUTURE WORKS

In this paper, an automated calibration system is demonstrated for a fingernail imaging system which predicts finger forces by taking images of fingernail. In order to apply forces and torques, two inexpensive Novint Falcon devices are connected by a rigid link which thus has 5 degrees of freedom. The system is able to simultaneously control 4-D force/torque, a normal force and a rotational torque in z direction, and two axes shear forces in x and y directions, with a settling time of less than 0.25 seconds on human fingerpad. Comparing with the calibration system presented previously in Ref. [3], this system provides slightly better control results for all three directions of force with a fraction of the cost. More importantly, this system is the first calibration system that is capable to apply the torque in normal direction along with forces in all three directions. This system will not only be very useful for calibration in finger force imaging technique, but also be able to extend many fingertip contact research [8] to higher dimensions. Furthermore, the system can be used for haptic rendering with or without force sensor.

Although the system has the ability to control the rotational torque in y direction, when the calibration system

applies on a human fingertip, the rotational torque in y direction is no longer controllable with current setup. It is very difficult to align the rotation axis on the fingertip and the force sensor due to the slippage and rolling between the fingertip and the force sensor, and deformation in the fingerpad. If the contact point is off the center of the force sensor, it will bring large errors to the feedback. Moreover, a tiny error of T_y will lead to a big rotation around y axis, so it has tremendous influence on system stability.

During the calibration stage, two force trajectories are designed for fast and sufficient calibrations. We split one 4-D force trajectory into one 3-D trajectory and one 2-D trajectory to reduce the complexity of one trajectory otherwise the sampling points would increase exponentially, which would require unreasonable time to finish the calibration. Experiments demonstrated that the system tracked the trajectories with an interval of 0.3 seconds, and step sizes of 0.1 N and 1 N·mm. The RMSE of tracking The RMSE is 0.04 N in F_x , 0.02 N in F_y , 0.03 N in F_z , and 0.39 N·mm in T_z .

In the future, we plan to investigate a feasible way to control the rotational torques for x and y directions also. We plan to use the camera system to provide more accurate position feedback for the fingertip to compute the real torque on the fingertip other than just relying on the force sensor feedback. In addition, we will explore new sampling techniques to fully explore a high dimensional space without increasing the number of samples.

VI. ACKNOWLEDGMENTS

This research was supported by the University of South Florida Seed Grant.

REFERENCES

- [1] P. Berkelman and R. Hollis. Lorentz magnetic levitation for haptic interaction: device design, function, and integration with simulated environments. *Intl J Robotics Research*, 9:644–667, 2000.
- [2] CMU. *Magnetic Levitation Haptic Interface User Manual*. 2008.
- [3] T. Grieve, Y. Sun, J. M. Hollerbach, and S. A. Mascaro. 3-d force control on the human fingerpad using a magnetic levitation device for fingernail imaging calibration. *EuroHaptics conference, 2009 and Symposium on Haptic Interfaces for Virtual Environment and Teleoperator Systems. World Haptics 2009. Third Joint*, pages 411–416, mar. 2009.
- [4] H. Kinoshita, L. Backstrom, J. R. Flanagan, and R. S. Johansson. Tangential Torque Effects on the Control of Grip Forces When Holding Objects With a Precision Grip. *J Neurophysiol*, 78(3):1619–1630, 1997.
- [5] S. A. Mascaro and H. H. Asada. Measurement of finger posture and three-axis fingertip touch force using fingernail sensors. *Robotics and Automation, IEEE Transactions on*, 20(1):26 – 35, 2004.
- [6] S. N. Norman. *Control Systems Engineering*. Wiley, 4th edition, 2003.
- [7] Inc. Novint Technologies. Technical specifications. 2007.
- [8] D. T. V. Pawluk and R. D. Howe. Dynamic contact mechanics of the human fingerpad against a flat surface. *ASME J. Biomed. Eng.*, 121:178–183, 1999.
- [9] Y. Sun, J. M. Hollerbach, and S. A. Mascaro. Measuring fingertip forces by imaging the fingernail. In *Proc 14th Symposium on Haptic Interfaces for Virtual Environment and Teleoperator Systems*, pages 125–131, Washington, DC, USA, 2006.
- [10] Y. Sun, J. M. Hollerbach, and S. A. Mascaro. Predicting fingertip forces by imaging coloration changes in the fingernail and surrounding skin. *IEEE Transactions on Biomedical Engineering*, 55(10):2363–2371, 2008.